Research Article | Vol. 27, No. 13 | 24 Jun 2019 | OPTICS EXPRESS 17667
Optics EXPRESS

Extracting optical constants of solid materials with micro-rough surfaces from ellipsometry without using effective medium approximation

YUANBIN LIU,[1,3] JUN QIU,[1,4,5] LINHUA LIU,[1,2,*] BINGYANG CAO[3,6]

[1]School of Energy Science and Engineering, Harbin Institute of Technology, 92, West Dazhi Street, Harbin 150001, China
[2]School of Energy and Power Engineering, Shandong University, Qingdao 266237, China
[3]Key Laboratory for Thermal Science and Power Engineering of Ministry of Education, Department of Engineering Mechanics, Tsinghua University, Beijing 100084, China
[4]State Key Lab of Digital Manufacturing Equipment and Technology, Huazhong University of Science and Technology, Wuhan, Hubei 430074, China
[5]qiujun8326@163.com
[6]caoby@tsinghua.edu.cn
*lhliu@hit.edu.cn

Abstract: The effective medium approximation (EMA) model may cause a large deviation in the data analysis of spectroscopic ellipsometry (SE) for solid materials with randomly micro-rough surfaces since it ignores the influence of the lateral irregularities of the rough surfaces on the electromagnetic scattering. In this work, a novel inversion framework is developed to extract optical constants from the SE parameters for solid materials with randomly micro-rough surfaces. Our approach enables the integration of the Levenberg-Marquardt optimization algorithm and the first-principles calculations of electromagnetic scattering. In each iterative step, the electromagnetic interactions with rough surfaces are accurately obtained from first-principles calculations without using the EMA model for rough estimation, which significantly guarantees the precision and wide applicability of our method for actual surfaces without a perfectly Gaussian height distribution. Furthermore, a superior advantage of our approach is that its error can be feasibly evaluated from the instrumental errors of the surface morphology detectors and the SE.

1. Introduction

The optical constants of materials are essential data and closely connected with many fields, such as photocatalysis [1,2], the solar desalination of sea water [3,4], thermophotovolatic emitters [5,6], and thin film materials in photonics [7,8]. The spectroscopic ellipsometry (SE) technique is well known as a powerful tool for evaluating the optical constants of solid samples due to its fast, precise, and non-destructive capabilities [9–12]. Using SE measurements, one can directly obtain the amplitude ratio Ψ and the phase difference Δ between the *p*- and *s*-polarizations of reflection light. The measured values (Ψ, Δ) are called the ellipsometric parameters and they are defined by [13]

$$\rho = \tan\Psi \exp(i\Delta) = \frac{r_p}{r_s}, \tag{1}$$

where ρ is the ellipsometric ratio, and r_p and r_s are the Fresnel reflection coefficients in the *p*- and *s*-polarizations, respectively. In the general data analysis of SE, by combining Eq. (1) and the Fresnel equations, the ellipsometry data can be transformed into the optical constants:

#361666 https://doi.org/10.1364/OE.27.017667
Journal © 2019 Received 20 Mar 2019; revised 25 May 2019; accepted 27 May 2019; published 12 Jun 2019

Optics EXPRESS

$$n - ik = \left\{ \left[\frac{(1-\rho)\sin^2\theta}{(1+\rho)\cos\theta} \right]^2 + \sin^2\theta \right\}^{1/2} \tag{2}$$

where n is the refractive index and k is the extinction coefficient of materials, and θ is the incident angle of light. It should be noted that the condition for using Eq. (2) is that sample surfaces have to be perfectly smooth, because the Fresnel equations describe only the reflection properties of such surfaces. Hence, samples with smooth surfaces are strongly recommended in the measurement of SE. However, any practical surface inevitably exhibits some roughness no matter how carefully it is polished. Although the referred surface roughness is usually much smaller than the wavelength of incident light in practical experiments, SE is capable of detecting the large deviation between ellipsometric responses from micro-rough and smooth surfaces since it is highly sensitive to surface structures [14–16]. Actually, such a deviation will yield pseudo optical constants. To obtain optical constants of samples that are more accurate, one may take into account the influence of rough surfaces on the electromagnetic scattering. A commonly considered method for this involves building the effective medium approximation (EMA) model to estimate the optical response of rough surfaces [13,17–19]. To use the EMA model, a surface's rough layer is replaced by a homogeneous and flat layer with an effective thickness and an effective dielectric function. As is usually done in an experimental data analysis, the thickness of the EMA layer is assumed to be equal to the root mean square height, which can be estimated from the surface morphology detectors, such as atomic force microscopy (AFM) [20]. In addition, the effective dielectric function is usually solved using Bruggeman's EMA theory.

Demonstrably, the EMA model cannot build the accurate mappings between the optical constants and the SE parameters, because it considers only the height irregularities and it neglects the large effect of the lateral characteristic dimensions on the electromagnetic scattering from rough surfaces. More details regarding the limitations of the EMA model can be found in our previous work [15]. Accordingly, the EMA model cannot easily satisfy the demands of high-precision measurements for optical constants. Conversely, the SE parameters can be precisely correlated with the optical constants by the first-principles calculations of Maxwell's equations [21–23]. In the past, the first-principles calculations of the electromagnetic scattering from rough surfaces were challengeable due to the limitations of computer memory and the consumption of a large amount of calculation time. With the remarkable progress of computers today, first-principles calculations of Maxwell's equations have been able to become crucial tools in the data analysis of SE for rough surfaces [24].

By combining the first-principles calculations of electromagnetic scattering and the Levenberg-Marquardt optimization algorithm, we present a novel inversion method to obtain the optical constants of solid materials with micro-rough surfaces from SE measurements. The error analysis of the proposed method is also introduced. Our approach uses the first-principles calculations of electromagnetic scattering to generate the mappings between the SE parameters and optical constants for micro-rough surfaces with various morphologies. In fact, there are many distribution forms of rough surfaces including random and periodic ones. Here, we adopted silicon samples with different Gaussian distributed randomly micro-rough surfaces to perform the theoretical verification of our method, because the Gaussian distribution is the most common and typical distribution [25]. Real sample surfaces may have no perfectly Gaussian distributions. Even so, due to the applicability of the first-principles calculations of electromagnetic scattering for arbitrary surface profiles, our method is not restricted to Gaussian distributed randomly micro-rough surfaces. In particular, gratings are generalized rough surfaces with periodic structures. In recent years, extracting the critical dimensions of gratings with SE has drawn extensive attention from researchers, who have accumulated abundant SE experimental data [26–29]. In the last part of this work, we

Optics EXPRESS

demonstrate the experimental validation of our method with the available SE experimental data for rectangular gratings and a real SiO_2 randomly rough surface.

2. Theoretical background and methodology

2.1 Gaussian distributed randomly micro-rough surface model

Generally, randomly micro-rough surfaces are characterized by the root mean square height σ and the correlation length ζ, which represent the vertical and lateral characteristic lengths of the randomly micro-rough surfaces, respectively. The correlation length ζ is defined by a lag length which drops from the peak value of the autocovariance function by a factor of e^{-1} [25]. As to Gaussian distributed randomly rough surfaces, the corresponding autocovariance function has the equivalent form [30]:

$$\left\langle H(\vec{p})H(\vec{p}+\vec{q})\right\rangle = \sigma^2 \exp\left[-\left(q^2/\zeta^2\right)\right] \tag{3}$$

where $H(\vec{p})$ represents the height at position $\vec{p}$, $\vec{q}$ is a spatial vector, and q denotes its magnitude.

2.2 Effective medium approximation

Assuming that the ambient surrounding of the sample is air or vacuum, the Bruggeman formula takes the form [13]:

$$\gamma\frac{\varepsilon_n-\varepsilon_{eff}}{\varepsilon_n+2\varepsilon_{eff}}+(1-\gamma)\frac{\varepsilon_v-\varepsilon_{eff}}{\varepsilon_v+2\varepsilon_{eff}}=0 \tag{4}$$

where γ and ε_n represent the volume fraction and the dielectric function of the measured sample, respectively, ε_v is the dielectric function of void spaces, and ε_{eff} is the effective dielectric function of the rough layer. In most cases, γ is usually regarded as a constant 50% to calculate effective dielectric functions of the EMA layer [31].

2.3 Direct problem

Consider a direct problem to solve the SE parameters of micro-rough surfaces. The SE parameter Ψ or Δ can be regarded as a function of several variables, including θ, λ, n, k, and the morphological parameters of surfaces, where λ denotes the wavelength of the incident light. For Gaussian distributed randomly micro-rough surfaces, the morphological parameters are σ and ζ. For rectangular gratings, the morphological parameters become the depth h, the line width b, and the period Λ. When the quantities of those variables are known, Ψ and Δ can be obtained from the first-principles calculation methods of electromagnetic scattering, such as the rigorous coupled-wave analysis (RCWA) [32,33], the finite-element method (FEM) [34], and the finite-difference time-domain (FDTD) method [23,35]. In this work, the FDTD method was employed to simulate the interaction of the electromagnetic wave with Gaussian distributed randomly micro-rough surfaces, while RCWA was used to calculate the electromagnetic response of rectangular gratings. Previously, Lehner et al. [35] applied FDTD to calculate the polarization optical response of randomly rough surfaces, and it is indicated that the electromagnetic response of a sample surface with arbitrary surface structure can be simulated with FDTD. In addition, in our recent work, we performed an experimental verification of the FDTD method on a two-dimensional SiO_2 randomly rough surface, and the simulated results agreed well with the experimental results [23]. The general procedures for obtaining the SE parameters with FDTD are as follows. First, FDTD is used to calculate the electric and magnetic fields within a finite space around the sample. Then the near-field to far-field transformation theory is applied to obtain the scattered fields in the region that is far away from the sample. Finally, the SE parameters are calculated from Eq. (1) based on the

Optics EXPRESS

scattered far field. The more detailed algorithms for FDTD and RCWA can be found in some references [36–39].

2.4 Inverse problem

For the inverse problem, the optical constants n and k are regarded as unknown, but the other quantities Ψ, Δ, θ, λ, and the morphological parameters of the surfaces are known. Among these quantities, the SE parameters are available from the SE experiment and the characteristic parameters of the surface morphology are estimated from the surface morphology detectors, such as AFM. When λ and the morphological parameters are unchanged, the SE parameters Ψ and Δ with respect to n and k are defined as follows:

$$\Psi = \Psi(\theta, n, k), \quad \Delta = \Delta(\theta, n, k). \tag{5}$$

In the inverse analysis, the optical constants are estimated by utilizing the measured SE parameters. To avoid the non-uniqueness of inversion, multiple sets of SE parameters may be adopted at different incident angles to build over-determined equations. Thus, the inverse problem of estimating the optical constants can be formulated as an optimization problem for the minimization of the objective function:

$$M(n,k) = \frac{1}{2}\sum_{i=1}^{m}\left\{\left[\Psi(\theta_i,n,k) - \Psi^*(\theta_i,n,k)\right]^2 + \left[\Delta(\theta_i,n,k) - \Delta^*(\theta_i,n,k)\right]^2\right\} \tag{6}$$

where Ψ^* and Δ^* represent the measured data, Ψ and Δ are the estimated SE parameters obtained from the solution of the direct problem based on the estimated optical constants (n, k), and m denotes the number of incident angles for monochromatic light.

2.5. Iterative method of minimization

Based on the Levenberg-Marquardt optimization algorithm, the following iterations are built to determine the unknown optical constants:

$$\begin{bmatrix} n_{j+1} \\ k_{j+1} \end{bmatrix} = \begin{bmatrix} n_j \\ k_j \end{bmatrix} - \alpha_i \left[J(n_j,k_j)^T J(n_j,k_j) + \mu_t I \right]^{-1} J(n_j,k_j)^T M(n_j,k_j), \quad j = 0, 1, 2, \ldots, \tag{7}$$

where the symbol '[]' represents a matrix, the subscript j denotes the number of iterations, α_i denotes the iteration step that can be determined by the Armijo search algorithm, μ_t is the iteration parameter, I is the 2×2 identity matrix, and J is the Jacobi matrix of the objective function M that takes the form

Optics EXPRESS

$$J(n_j,k_j)=\begin{bmatrix} \frac{\partial\Psi(\theta_1,n_j,k_j)}{n_j} & \frac{\partial\Psi(\theta_1,n_j,k_j)}{k_j} \\ \vdots & \vdots \\ \frac{\partial\Psi(\theta_i,n_j,k_j)}{n_j} & \frac{\partial\Psi(\theta_i,n_j,k_j)}{k_j} \\ \vdots & \vdots \\ \frac{\partial\Psi(\theta_m,n_j,k_j)}{n_j} & \frac{\partial\Psi(\theta_m,n_j,k_j)}{k_j} \\ \frac{\partial\Delta(\theta_1,n_j,k_j)}{n_j} & \frac{\partial\Delta(\theta_1,n_j,k_j)}{k_j} \\ \vdots & \vdots \\ \frac{\partial\Delta(\theta_i,n_j,k_j)}{n_j} & \frac{\partial\Delta(\theta_i,n_j,k_j)}{k_j} \\ \vdots & \vdots \\ \frac{\partial\Delta(\theta_m,n_j,k_j)}{n_j} & \frac{\partial\Delta(\theta_m,n_j,k_j)}{k_j} \end{bmatrix}, \quad i=1,2,...,m. \tag{8}$$

In Eq. (8), the difference approximations are taken for the partial derivatives. The termination criterion of iteration is selected in the following manner:

$$M(n_j,k_j)<\frac{m}{2}\left[(\delta\Psi)^2+(\delta\Delta)^2\right], \quad j=1,2,3... \tag{9}$$

where $\delta\Psi$ and $\delta\Delta$ denote the standard deviations of the measurement errors of Ψ and Δ, respectively.

The computational procedure of the inversion method can be summarized as follows:

Step 1. Choose the initial guess (n_0 , k_0). This work provides two methods for producing the initial guess. The first method involves regarding the pseudo optical constants (n_p , k_p) calculated by Eq. (2) as the initial guess. In fact, when the relative roughness of the micro-rough surfaces is rather small and ζ is relatively large, the pseudo optical constants are quite close to (n^*, k^*). Another way for obtaining (n_0 , k_0) involves the use of the EMA model. Based on an EMA model with a thickness of σ, another initial guess can be obtained as (n_E , k_E).

Step 2. Knowing (n_0 , k_0) and the incident angle, solve the direct problem and calculate the objective function defined by Eq. (6). Stop the iteration process, if the termination criterion is satisfied. Otherwise, go to **Step 3**.

Step 3. Give the differential step sizes of n and k to calculate $J(n_0,k_0)$.

Step 4. Determine α_i with the Armijo algorithm and compute the iteration equation given by Eq. (7).

Step 5. Solve the direct problem and calculate the objective function defined by Eq. (6). Stop the iteration process if the termination criterion is satisfied. Otherwise, go to **Step 6**.

Step 6. Set $j=j+1$ and compute $J(n_j,k_j)$. Then go back to **Step 4**.

The error of the inversion method depends on the measurement errors of the instruments, including the SE and surface morphology detectors. For the Gaussian distributed randomly micro-rough surfaces, the standard deviations (δn, δk) of the optical constants of a sample can be estimated from the following equations:

Optics EXPRESS

$$\delta n = \sqrt{\left(\frac{\partial n}{\partial \sigma}\delta\sigma\right)^2 + \left(\frac{\partial n}{\partial \zeta}\delta\zeta\right)^2 + \left(\frac{\partial n}{\partial \Delta}\delta\Delta\right)^2 + \left(\frac{\partial n}{\partial \Psi}\delta\Psi\right)^2} \quad (10a)$$

$$\delta k = \sqrt{\left(\frac{\partial k}{\partial \sigma}\delta\sigma\right)^2 + \left(\frac{\partial k}{\partial \zeta}\delta\zeta\right)^2 + \left(\frac{\partial k}{\partial \Delta}\delta\Delta\right)^2 + \left(\frac{\partial k}{\partial \Psi}\delta\Psi\right)^2} \quad (10b)$$

where $\delta\sigma$ and $\delta\zeta$ denote the standard deviations of the measurement errors of the surface morphology detectors in the vertical and lateral dimensions, respectively. The partial derivatives in Eq. (10) can be calculated using the first-principles calculations of the electromagnetic scattering and difference approximations. Compared with the EMA model, great progress is made in the fact that the error of the inversion method can be estimated from Eq. (10).

3. Results and discussion

Based on the proposed inversion method, several examples of the analysis of the SE parameters are presented in this section. It is impossible to provide the analysis of all types of samples. To make the inversion method well understood, a detailed example is shown first including complete procedures. Then more examples are exhibited for different morphologies, which are used to validate the feasibility of the proposed method.

3.1 A detailed case

In the case of no measurement errors of the surface morphology and the SE parameters, the first detailed example was performed for a silicon wafer with Gaussian distributed randomly micro-rough surfaces. The wavelength of light was selected as 400 nm and the incident angle was chosen as 60°. As aforementioned, one may use various incident angles to avoid the non-uniqueness of inversion. For Gaussian micro-rough surfaces, however, adopting an incident angle is generally enough due to randomness. The assumed root mean square height is σ = 10 nm and the correlation length is ζ = 50 nm. At first, we obtained the optical constants of Si from [40] and checked the grid independence of the FDTD simulation, as shown in Fig. 1. Based on the convergence of calculations, a mesh size of λ/400 was used for this case, which could reproduce the morphology of the rough surfaces well. It is worth noting that different mesh sizes for various morphologies was used to guarantee the grid independence of the simulation.

The n - k and Ψ - Δ trajectories of the iteration are shown in Fig. 2. The true optical constants and the "measured" SE parameters were marked with the pentagram plotted in Fig. 2(a) and 2(b), respectively. They served as the benchmarks for verifying the inversion method. The "measured" SE parameters were simulated by FDTD based on the true optical constants. The digits in Fig. 2 represent the positions of the optical constants and the corresponding SE parameters after the jth iteration. According to the procedure of the inversion method, the pseudo optical constants labeled with 'S' in Fig. 2(a) were chosen as the initial guess or the starting point of iteration. Figure 2(a) illustrates the fact that the pseudo optical constants had an obvious deviation from the true optical constants, which again indicated that the surface roughness had a significant effect on the SE measurement. By solving the direct problem, the corresponding SE parameters at the initial guess (n_0 , k_0) could be obtained from the FDTD simulation for the same rough surface. These parameters are shown in Fig. 2(b). Then we set the differential step sizes of n and k as 0.0001 to calculate $J(n_0, k_0)$ using the difference approximations. The first iterative results labeled with '1' were obtained by solving Eq. (7). At the time, the termination criterion Eq. (9) was not satisfied. Hence, the iterations were executed continuously based on **Step 4** to **6** until the termination criterion was met. It was worth noting that although the FDTD simulations usually generated

Optics EXPRESS

the highly reliable results at the expense of long simulation time, the advantage of our approach was its robustness and fast convergence speed, which saved a lot of computation time. As shown in Fig. 2, after five iterations, the optical constants obtained from the inversion method were almost equal to the true values. At the time, the objective function was less than 5×10^{-3}. For other cases, the convergence speed was similar with that in Fig. 2. All computations in this work were carried out on a PC with 2.7 GHz processor (Intel(R) Xeon(R) Platinum 8168 CPU) and 383 GB RAM. An entire inversion process took about 5 hours.

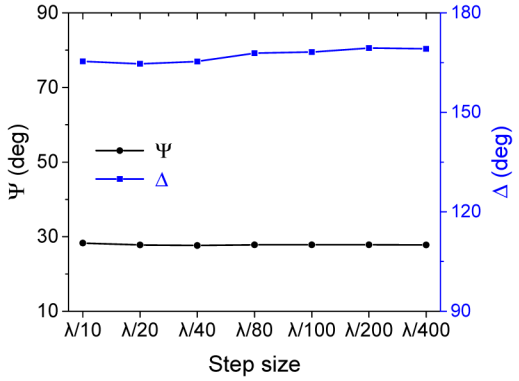

Fig. 1. Check of the grid independence of the FDTD simulation for the Gaussian distributed randomly micro-rough surfaces: $\sigma = 10$ nm and $\zeta = 50$ nm.

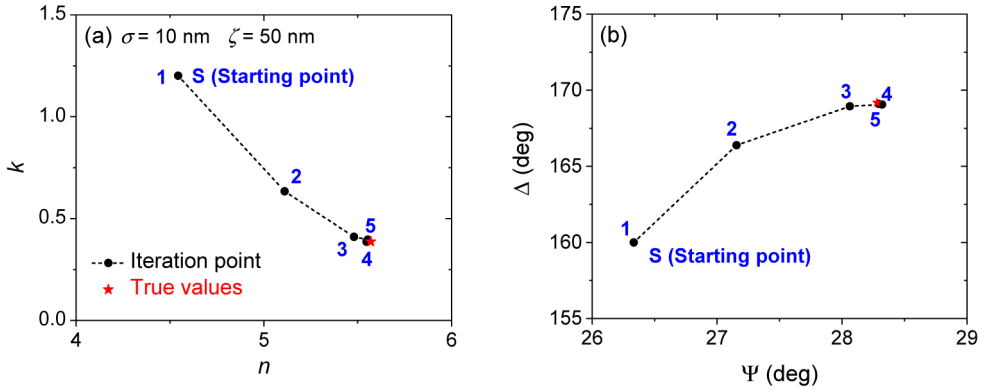

Fig. 2. (a) n - k and (b) Ψ - Δ trajectories of the iteration operated in a silicon wafer with the Gaussian distributed randomly micro-rough surfaces of $\sigma = 10$ nm and $\zeta = 50$ nm ($\lambda = 400$ nm, $\theta = 60°$).

3.2. Spectroscopic results for different surface morphologies

After describing a detailed case, this section will demonstrate the applicability of the proposed inversion method for different rough surfaces at various incident wavelengths. The results are shown in Fig. 3. The spectroscopic range was chosen from 400 nm to 1000 nm and the incident angle was 60°. The studied material in this section is still Si. The morphological parameters were $\sigma = 10$ nm and $\zeta = 50$ nm in Figs. 3(a) and 3(b), while the parameters were $\sigma = 20$ nm and $\zeta = 40$ nm in Figs. 3(c) and 3(d). The results corresponded to three analysis methods to obtain the optical constants from the SE parameters. The first method was utilizing the Fresnel equations of the smooth surfaces to obtain pseudo optical constants. The second and the last methods involved performing the data analysis with the EMA model and the proposed inversion method, respectively. It was shown that our inversion approach

Optics EXPRESS

performed with the highest precision among the above three methods. All of the inversion results produced by our method agreed well with the true optical constants obtained from [40].

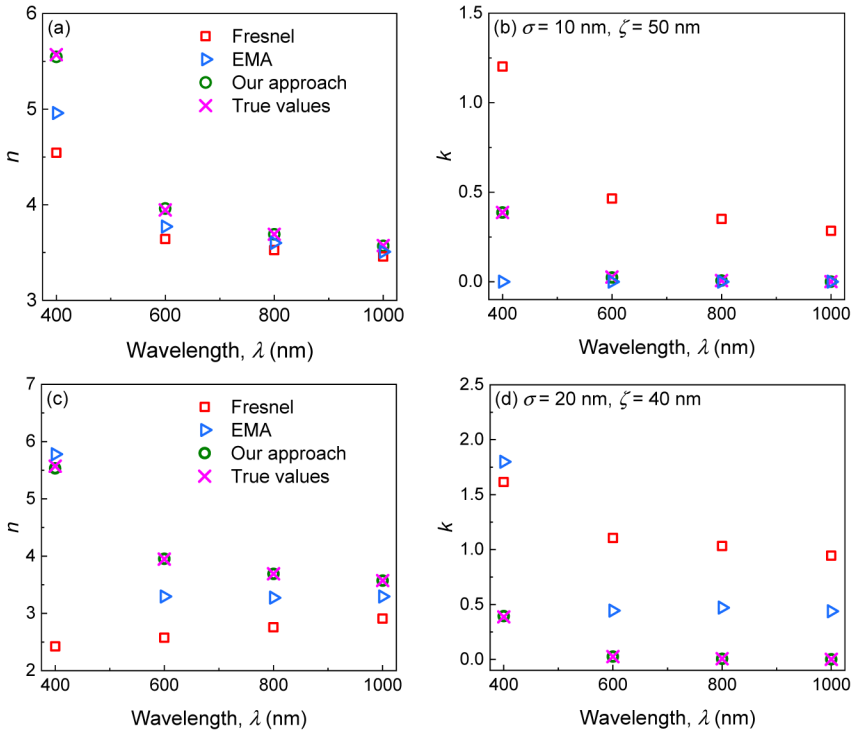

Fig. 3. Optical constants of Si with the Gaussian distributed randomly micro-rough surfaces estimated from the SE parameters using the Fresnel equations, the EMA model, and our inversion method, respectively. The morphological parameters were σ = 10 nm and ζ = 50 nm for subfigures (a) and (b), while the parameters were σ = 20 nm and ζ = 40 nm for subfigures (c) and (d). The incident angle was θ = 60°. The true values of the optical constants were obtained from [40].

The error comparison of the three analysis methods used to obtain the optical constants is shown in Table 1. We define the relative error of complex refractive index as

$$\alpha = \sqrt{\frac{\left(n-n^*\right)^2+\left(k-k^*\right)^2}{\left(n^*\right)^2+\left(k^*\right)^2}} \times 100\%. \tag{11}$$

As presented in Table 1, the optical constants obtained from the Fresnel equations of the smooth surfaces deviated further from the true values when σ/λ increased. Compared with the Fresnel equations, the EMA model was capable of obtaining more reliable results. Similarly, the precision of the EMA model went up with the decreasing σ/λ. For the inversion method, those results were obtained within five iterations. All of the cases in Table 1 illustrate the robust convergence and the high-precision results of the inversion method for different morphologies and wavelengths. The main reason for this was that the electromagnetic interaction of light with the rough surfaces was accurately obtained from the first-principles calculations of Maxwell's equations in each iterative step.

To check the influence of the measurement errors of the SE parameters and the surface morphologies on the inversion method, four cases were chosen from Table 1. The standard deviations of the optical constants in the error transfer formula Eq. (10) are presented in Table

Optics EXPRESS

2. The coefficients in Eq. (10) could be readily solved by numerical difference calculations. Based on the measurement errors of AFM and SE, the standard deviations could be computed. Generally, for the visible variable angle spectroscopic ellipsometry (V-VASE), the errors were $|\delta\Psi| = 0.03°$ and $|\delta\Delta| = 0.2°$ [41]. We assumed that the errors of AFM were less than 0.5% of the characteristic lengths, which could be completely guaranteed by current devices. Substituting these parameters and coefficients into Eq. (10), the standard deviations of the optical constants caused by the instrumental errors were calculated. The results show that the measurement errors of AFM and SE had an evident effect on the inversion method due to the strong sensitivity of the SE measurements.

Table 1. Error comparison of the Fresnel equations, the EMA model, and the inversion method used to obtain the optical constants of Si in the case of no measurement errors.

Morphologies (nm)		Wavelength (nm)	Fresnel equations	EMA	Inversion method
σ	ζ	λ	α	α	α
10	50	400	23.47%	12.94%	0.41%
10	50	600	13.53%	4.46%	0.37%
10	50	800	10.36%	2.44%	0.01%
10	50	1000	8.58%	1.85%	0.12%
20	40	400	60.46%	25.56%	0.68%
20	40	600	44.22%	19.63%	0.14%
20	40	800	37.54%	16.90%	0.04%
20	40	1000	32.30%	14.49%	0.00%

Table 2. Standard deviations of the optical constants caused by the instrumental errors of AFM and SE.

Morphologies (nm)		δn	δk
σ	ζ		
10	50	0.0076	0.0414
		0.1227	0.0544
		0.2124	0.0943
		0.1822	0.0833

3.3. Experimental validation

Gratings are special rough surfaces with periodic structures. Figure 4 shows the schematic of the 1D rectangular grating. In this section, we employ some available SE experimental data for gratings to verify the validation of our approach. The experimental data were retrieved from [29] and these data are shown in Fig. 5. In the reference literature, the chosen samples were rectangular-relief Si gratings patterned on a Si substrate. The incident angle was 65.45° in the measurement. The critical dimensions used in the present study were $\Lambda = 134.1$ nm, $b = 47.1$ nm, and $h = 116.7$ nm. The technical details of the relative apparatus can be found in the literature [29]. In this work, RCWA was employed to calculate the electromagnetic response of the 1D rectangular grating. The numerical accuracy of RCWA was significantly influenced by the number of the diffraction orders. To yield accurate results using a reasonable amount

Optics EXPRESS

of time, the number of diffraction orders was determined as 501 with a convergence check. Si is a well-known material and the reference data for its optical constants were obtained from [40]. Based on the known optical constants, the accuracy of our RCWA simulation was checked by comparing it with the available experimental data, as illustrated in Fig. 5. Simultaneously, the good fitting results demonstrate the reasonability of choosing these reference data as the benchmark of the optical constants in the process of verifying our method.

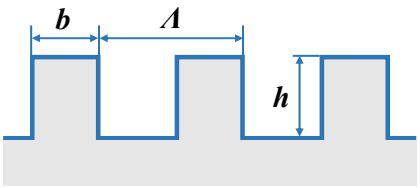

Fig. 4. Schematic of the 1D grating nanostructure. As found in [29], the geometric parameters used in the present study are Λ = 134.1 nm, b = 47.1 nm, and h = 116.7 nm.

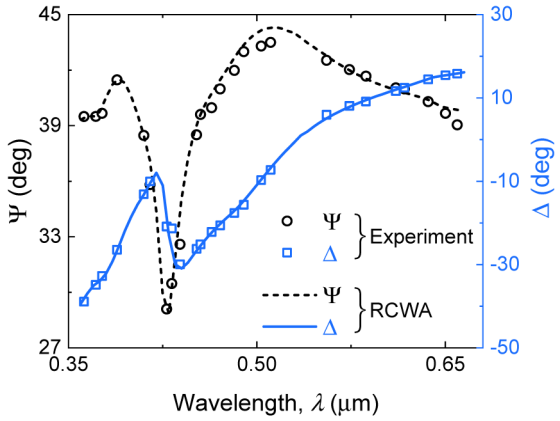

Fig. 5. Comparison of the SE parameters yielded from our RCWA simulation with experimental results in [29].

Before checking the validation of our approach, we investigated the accuracy of the EMA model for the optical constants inversion for gratings. In the inversion process, the film thickness of the EMA layer was taken as the grating height (h = 116.7 nm) and the grating duty cycle was 35.12%. The comparison of the inversion from the EMA model with the reference data is shown in Fig. 6(a). This comparison implies that the EMA model failed to predict the optical constants of samples with grating structures.

Our inversion method was then checked using the same case. In fact, due to the periodicity of the gratings, it was possible to yield identical SE parameters at the same incident angle for two samples with the different optical constants and with same grating dimensions. To overcome this challenge, our strategy involved performing the inversion method in sequence from the shortest wavelength to the longest wavelength, not simultaneously conducting the inversion over the entire spectrum. First, we provided an initial guess n_0 = 5 and k_0 = 1 for the shortest wavelength, which was not close to but not far away from the reference data. Later, we could obtain the final inversion results at the shortest wavelength. When dealing with the second wavelength, the initial guess might be taken as the inversion results corresponding to the first wavelength. In a similar way, the inversion results for the last wavelength acted as the initial guess for the next wavelength. The advantage achieved with this method was the guarantee that the initial guess at the next wavelength could not be far away from the true values due to the continuity of the optical constants. As a

Optics EXPRESS

result, Fig. 6(b) shows that the results derived from our approach agreed well with the reference data. In the entire inversion process, we only assumed the first initial guess at the shortest wavelength. This was a fair way to verify the validation of our approach. The deviation of the inversion results from the experiment was probably due to the deviations of the shape of the grating lines from perfectly vertical structures.

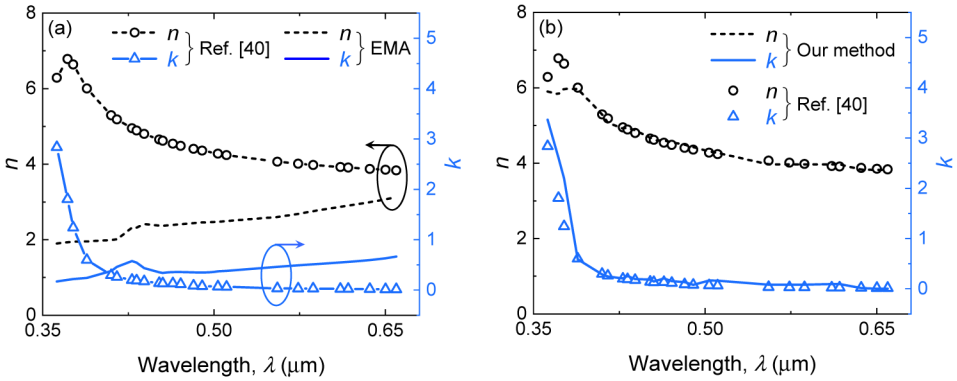

Fig. 6. Comparisons of the reference data of Si with the optical constants obtained from (a) the EMA model and (b) our inversion method.

Furthermore, we conducted an experimental validation of our approach on a real SiO_2 rough surface. The experimental data about the rough sample were directly retrieved from our previous work [23]. The surface geometrical morphology was scanned by Bruker Dimension FastScan AFM as shown in Fig. 7. The measured morphological parameters were σ = 0.462 μm and ζ = 2.78 μm. More experimental details could be found in the literature [23]. The errors AFM were less than 0.5% of the characteristic lengths. For the wavelength range from 2 to 30 μm, the errors of the employed ellipsometer are $|\delta\Psi|$ = 0.1° and $|\delta\Delta|$ = 0.5°. We randomly chose three target wavelengths of 7.81, 9.97, and 12.71 μm to extract their corresponding optical constants via our inversion method. The initial guess (n_0, k_0) for the wavelengths of 7.81, 9.97, and 12.71 μm were also discretionarily chosen as (2, 1), (3.55, 0.97), and (3, 1.5), respectively. As shown in Table 3, good agreement of the reference data with the optical constants obtained from our method validates the accuracy of our method. Additionally, the standard deviations of the optical constants caused by the instrumental errors were calculated in Table 3. The slight deviation of the optical constants obtained from our method from the reference data might mainly arise from the impurities of the sample and the statistical errors of the Gaussian distribution.

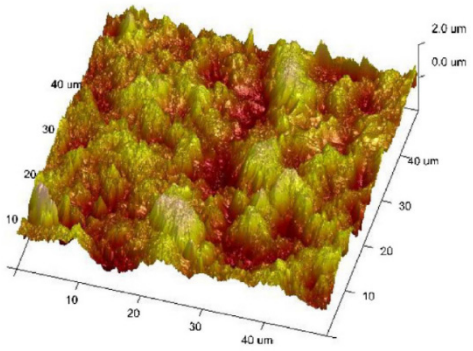

Fig. 7. Morphology of the SiO_2 rough surface scanned by AFM, which was obtained from the literature [23]. The statistically morphological parameters were σ = 0.462 μm and ζ = 2.78 μm.

Optics EXPRESS

Table 3. Comparison of the reference data of SiO_2 with the optical constants obtained from our inversion method. Here δn and δk are standard deviations of the optical constants caused by the instrumental errors of AFM and SE.

Wavelength (μm)	Reference data [40]		Our inversion method		Relative error
λ	n	k	n (δn)	k (δk)	α
7.81	0.6292	0.0744	0.6468(0.0049)	0.0791(0.0075)	2.88%
9.97	2.7080	0.5648	2.5058(0.0419)	0.5510(0.0400)	7.33%
12.71	1.7956	0.3021	1.7603(0.0162)	0.2984(0.0149)	1.95%

4. Conclusions

The EMA model cannot build accurate mappings between the optical constants and the SE parameters for micro-rough surfaces since it neglects the large effect of the correlation length on the electromagnetic scattering from rough surfaces. This may cause the large deviation of optical constants in the data analysis of SE. Additionally, the precision of the EMA model is difficult to evaluate quantitatively. In this paper, based on the first-principles calculations of Maxwell's equations and the Levenberg-Marquardt optimization algorithm, a novel inversion method is proposed to obtain optical constants of solid materials with randomly micro-rough surfaces. First, the samples with different Gaussian distributed randomly micro-rough surfaces were employed to theoretically verify the accuracy of the inversion method. All of the results suggest that the method had a robust convergence and a higher precision than the EMA model. The error of the inversion method was estimated by the measurement errors of SE and surface morphology detectors (such as AFM), which had a superior advantage to the EMA model. In addition to the numerical verification, the experimental validation of our method was also conducted with the available SE experimental data of rectangular gratings and a real SiO_2 randomly rough surface. Overall, the EMA model was always a tool that people relied on to perform the data analysis of SE for rough surfaces, but this work provides another method with wider applicability and higher precision.

Funding

National Natural Science Foundation of China (51336002, 51825601, 51621062).

References

1. K. Maeda, K. Teramura, D. Lu, T. Takata, N. Saito, Y. Inoue, and K. Domen, "Photocatalyst releasing hydrogen from water," Nature **440**(7082), 295 (2006).
2. X. Wang, C. Liow, D. Qi, B. Zhu, W. R. Leow, H. Wang, C. Xue, X. Chen, and S. Li, "Programmable Photo-Electrochemical Hydrogen Evolution Based on Multi-Segmented CdS-Au Nanorod Arrays," Adv. Mater. **26**(21), 3506–3512 (2014).
3. O. Neumann, A. S. Urban, J. Day, S. Lal, P. Nordlander, and N. J. Halas, "Solar Vapor Generation Enabled by Nanoparticles," ACS Nano **7**(1), 42–49 (2013).
4. L. Zhou, Y. Tan, J. Wang, W. Xu, Y. Yuan, W. Cai, S. Zhu, and J. Zhu, "3D self-assembly of aluminium nanoparticles for plasmon-enhanced solar desalination," Nat. Photonics **10**(6), 393–398 (2016).
5. Y. B. Liu, R. Jin, J. Qiu, and L. H. Liu, "Spectral radiative properties of a nickel porous microstructure and magnetic polariton resonance for light trapping," Int. J Heat Mass Transf. **98**, 833–844 (2016).
6. Y. Liu, J. Qiu, J. Zhao, and L. Liu, "General design method of ultra-broadband perfect absorbers based on magnetic polaritons," Opt. Express **25**(20), A980–A989 (2017).
7. A. Polman, "Erbium implanted thin film photonic materials," J. Appl. Phys. **82**(1), 1–39 (1997).
8. J. Q. Xi, M. F. Schubert, J. K. Kim, E. F. Schubert, M. Chen, S.-Y. Lin, W. Liu, and J. A. Smart, "Optical thin-film materials with low refractive index for broadband elimination of Fresnel reflection," Nat. Photonics **1**(3), 176–179 (2007).
9. L. Maria and H. Kurt, *Ellipsometry at the Nanoscale* (Springer, 2013).
10. X. G. Chen, Y. T. Shi, H. Jiang, C. W. Zhang, and S. Y. Liu, "Nondestructive analysis of lithographic patterns with natural line edge roughness from Mueller matrix ellipsometric data," Appl. Surf. Sci. **388**, 524–530 (2016).

Optics EXPRESS

11. M. Medikonda, G. R. Muthinti, R. Vasić, T. N. Adam, A. Reznicek, M. Wormington, G. Malladi, Y. Kim, Y.-C. Huang, and A. C. Diebold, "Optical properties of pseudomorphic Ge1−xSnx (x = 0 to 0.11) alloys on Ge(001)," J. Vac. Sci. Technol. B **32**(6), 061805 (2014).
12. S. Sunkoju, S. Schujman, D. Dixit, A. Diebold, J. Li, R. Collins, and P. Haldar, "Spectroscopic ellipsometry studies of 3-stage deposition of CuIn1−xGaxSe2 on Mo-coated glass and stainless steel substrates," Thin Solid Films **606**, 113–119 (2016).
13. H. Fujiwara, *Spectroscopic Ellipsometry: Principles and Applications* (John Wiley & Sons, 2007).
14. C. A. Fenstermaker and F. L. McCrackin, "Errors arising from surface roughness in ellipsometric measurement of the refractive index of a surface," Surf. Sci. **16**, 85–96 (1969).
15. Y. Liu, J. Qiu, and L. Liu, "Applicability of the effective medium approximation in the ellipsometry of randomly micro-rough solid surfaces," Opt. Express **26**(13), 16560–16571 (2018).
16. J. Mistrik, T. Yamaguchi, D. Franta, I. Ohlidal, G. J. Hu, and N. Dai, "Optical properties of rough LaNiO3 thin films studied by spectroscopic ellipsometry and reflectometry," Appl. Surf. Sci. **244**(1-4), 431–434 (2005).
17. D. E. Aspnes, J. B. Theeten, and F. Hottier, "Investigation of effective-medium models of microscopic surface roughness by spectroscopic ellipsometry," Phys. Rev. B Condens. Matter **20**(8), 3292–3302 (1979).
18. I. Ohlídal, J. Vohánka, M. Čermák, and D. Franta, "Optical characterization of randomly microrough surfaces covered with very thin overlayers using effective medium approximation and Rayleigh–Rice theory," Appl. Surf. Sci. **419**, 942–956 (2017).
19. D. Franta and I. Ohlídal, "Influence of lateral dimensions of the irregularities on the optical quantities of rough surfaces," J. Opt. A, Pure Appl. Opt. **8**(9), 763–774 (2006).
20. V. Sirtori, L. Magagnin, E. Saglia, and P. L. Cavallotti, "Calculation model of rough gold optical constants," Surf. Sci. **554**(2-3), 119–124 (2004).
21. H.-T. Huang and F. L. Terry, Jr., "Spectroscopic ellipsometry and reflectometry from gratings (Scatterometry) for critical dimension measurement and in situ, real-time process monitoring," Thin Solid Films **455–456**, 828–836 (2004).
22. B. Kaplan, T. Novikova, A. De Martino, and B. Drévillon, "Characterization of bidimensional gratings by spectroscopic ellipsometry and angle-resolved Mueller polarimetry," Appl. Opt. **43**(6), 1233–1240 (2004).
23. J. Qiu, D. F. Ran, Y. B. Liu, and L. H. Liu, "Investigation of ellipsometric parameters of 2D microrough surfaces by FDTD," Appl. Opt. **55**(20), 5423–5431 (2016).
24. M. I. Mishchenko, J. M. Dlugach, M. A. Yurkin, L. Bi, B. Cairns, L. Liu, R. L. Panetta, L. D. Travis, P. Yang, and N. T. Zakharova, "First-principles modeling of electromagnetic scattering by discrete and discretely heterogeneous random media," Phys. Rep. **632**, 1–75 (2016).
25. J. C. Stover, *Optical scattering: measurement and analysis* (SPIE, 2012).
26. J. Zhu, S. Liu, X. Chen, C. Zhang, and H. Jiang, "Robust solution to the inverse problem in optical scatterometry," Opt. Express **22**(18), 22031–22042 (2014).
27. S. Liu, W. Du, X. Chen, H. Jiang, and C. Zhang, "Mueller matrix imaging ellipsometry for nanostructure metrology," Opt. Express **23**(13), 17316–17329 (2015).
28. M. Foldyna, A. De Martino, E. Garcia-Caurel, R. Ossikovski, C. Licitra, F. Bertin, K. Postava, and B. Drevillon, "Critical dimension of biperiodic gratings determined by spectral ellipsometry and Mueller matrix polarimetry," Eur. Phys. J. Appl. Phys. **42**(3), 351–359 (2008).
29. R. Antos, J. Pistora, J. Mistrik, T. Yamaguchi, S. Yamaguchi, M. Horie, S. Visnovsky, and Y. Otani, "Convergence properties of critical dimension measurements by spectroscopic ellipsometry on gratings made of various materials," J. Appl. Phys. **100**(5), 054906 (2006).
30. D. Bergstrom, J. Powell, and A. F. H. Kaplan, "A ray-tracing analysis of the absorption of light by smooth and rough metal surfaces," J. Appl. Phys. **101**(11), 113504 (2007).
31. R. W. Collins, I. An, H. Fujiwara, J. C. Lee, Y. W. Lu, J. Y. Koh, and P. I. Rovira, "Advances in multichannel spectroscopic ellipsometry," Thin Solid Films **313**, 18–32 (1998).
32. W. J. Zhang, J. Qiu, and L. H. Liu, "Deviation characteristics of specular reflectivity of micro-rough surface from Fresnel′s equation," J. Quant. Spectrosc. Radiat. **160**, 50–62 (2015).
33. D. Dixit, S. O'Mullane, S. Sunkoju, A. Gottipati, E. R. Hosler, V. Kamineni, M. Preil, N. Keller, J. Race, G. R. Muthinti, and A. C. Diebold, "Sensitivity analysis and line edge roughness determination of 28-nm pitch silicon fins using Mueller matrix spectroscopic ellipsometry-based optical critical dimension metrology," J. Micro. Nanolithogr. MEMS MOEMS **14**(3), 031208 (2015).
34. B. Fodor, P. Kozma, S. Burger, M. Fried, and P. Petrik, "Effective medium approximation of ellipsometric response from random surface roughness simulated by finite-element method," Thin Solid Films **617**, 20–24 (2016).
35. B. Lehner and K. Hingerl, "The finite difference time domain method as a numerical tool for studying the polarization optical response of rough surfaces," Thin Solid Films **455**, 462–467 (2004).
36. D. Sullivan, *Electromagnetic Simulation Using the FDTD Method* (Wiley & Sons 2013).
37. A. Taflove and S. Hagness, *Computational electrodynamics: the finite-difference time-domain method* (Artech House, 2005).
38. G. Granet and B. Guizal, "Efficient implementation of the coupled-wave method for metallic lamellar gratings in TM polarization," J. Opt. Soc. Am. A **13**(5), 1019–1023 (1996).
39. L. Li and C. W. Haggans, "Convergence of the coupled-wave method for metallic lamellar diffraction gratings," J. Opt. Soc. Am. A **10**(6), 1184–1189 (1993).

Optics EXPRESS

40. E. D. Palik, *Handbook of Optical Constants of Solids* (Boston Academic, 1991).
41. H. H. U. Yang, J. D'Archangel, M. L. Sundheimer, E. Tucker, G. D. Boreman, and M. B. Raschke, "Optical dielectric function of silver," Phys. Rev. B Condens. Matter Mater. Phys. **91**(23), 235137 (2015).